Polymorphic crystalline wetting layers on crystal surfaces

Xipeng Wang
Hong Kong University of Science and Technology
Bo Li
Institute for Basic Science https://orcid.org/0000-0003-3596-5542
Mengmeng Li
Hong Kong University of Science and Technology
Yilong Han (yilong@ust.hk)
Hong Kong University of Science and Technology https://orcid.org/0000-0002-1439-0121

Article

Keywords:

Posted Date: October 14th, 2021

DOI: https://doi.org/10.21203/rs.3.rs-910546/v1

Polymorphic crystalline wetting layers on crystal surfaces

Xipeng Wang[1,2,3†], Bo Li[1†], Mengmeng Li[1] & Yilong Han[1,4*]
1 Department of Physics, The Hong Kong University of Science and Technology, Clear Water Bay, Hong Kong, China.
2 Beijing Computational Science Research Center, Beijing 100193, China.
3 Yusuf Hamied Department of Chemistry, University of Cambridge, Cambridge, CB2 1EW, UK.
4 The Hong Kong University of Science and Technology Shenzhen Research Institute, Shenzhen 518057, China. and
5 Center for Soft and Living Matter, Institute of Basic Science, Ulsan, South Korea.

Analogous to surface premelting, we propose that a crystal surface can undergo a pre-solid–solid transition, i.e. developing a thin polymorphic crystalline layer before reaching the solid–solid transition temperature if two crystals can form a low-energy coherent interface. We confirm this in simulations and colloid experiments at single-particle resolution. The power-law increase of surface layer thickness is analogous to premelting. Different kinetics and reversibilities of surface-crystal growth are observed in various systems. Surface crystals exist not only under thermal equilibrium, but also during melting, crystallization, and grain coarsening. Furthermore, the premelting and pre-solid–solid transition can coexist, resulting double surface wetting layers. We hypothesize that such surface phenomena exist in atomic and molecular crystals, which provide a novel way to tune material properties.

Most crystal surfaces can develop a thin layer of liquid slightly below its melting temperature. Such surface premelting is crucial to skating, glacier movement and snow formation [1, 2], and occurs when surface liquid can effectively wet bulk phases, i.e.

$$\gamma_{\mathrm{cv}} > \gamma_{\mathrm{cs}} + \gamma_{\mathrm{sv}}, \tag{1}$$

where γ is the interfacial energy, and the subscripts "cv", "cs" and "sv" represent the crystal–vapour, crystal–surface layer and surface layer–vapour interfaces, respectively. A surface-wetting layer can be any phase that satisfies inequality (1), i.e. the total energy of the newly formed two interfaces is lower than that of the original interface. A similar but less studied phenomenon is surface prefreezing, i.e. a liquid freezing into a thin crystalline layer on a flat substrate [3–5] or at a liquid–air interface [6] slightly above its crystallisation temperature. By analogy with premelting and prefreezing, we propose that a thin polymorphic crystalline layer can form on the surface of a crystal approaching its solid–solid (s–s) transition temperature or pressure, and use the term "pre-solid–solid transition" to describe this phenomenon. The s–s transition occurs between different polymorphic crystals composed of the same type of atoms or molecules, e.g. between diamond and graphite, which are both formed from carbon atoms. It would be highly useful if a thin layer of graphite could be controllably formed on or removed from a diamond surface by tuning temperature or pressure. Unfortunately, this is not possible in the graphite–diamond case, as their lattice mismatch leads to a high γ_{cs}, which cannot satisfy inequality (1). However, when the lattice constants, orientations and symmetries of polymorphic crystals are well matched, their two lattices can connect perfectly (Fig. 1a) and form a coherent interface. Such interface has an extremely low energy ($\gamma_{\mathrm{cs}} \simeq 0$). Thus, inequality (1) is easily satisfied when a surface crystal is less dense than a bulk crystal, i.e. closer to the density of the corresponding vapour, such that $\gamma_{\mathrm{cv}} > \gamma_{\mathrm{sv}}$. Furthermore, the above analysis holds if vapour is replaced by liquid. Thus, a polymorphic crystal layer can form on the surface of a bulk crystal in either vapour or liquid under thermal equilibrium, i.e. near either the vapour–crystal (Fig. S1) or the liquid–crystal coexistence line in its phase diagram.

Atoms on free surfaces of solids can rearrange into a structure different from the bulk, but such surface reconstruction usually occurs at only one layer of atoms and is not sensitive to the temperature change [7]. Consequently, surface reconstruction is not regarded as a precursor of phase transition or a surface wetting phenomenon such as premelting.

Neither premelting nor the formation of surface crystals are phase transitions. The latter is actually a precursor of the s–s transition, as it is a wetting phenomenon that occurs at thermal equilibrium, during which the bulk crystal remains the stable phase with the lowest chemical potential. We confirm the formation of surface crystals by experiment and simulation, and reveal their microscopic kinetics and roles in melting, crystallisation, s–s transition and polycrystalline annealing processes.

Colloids are outstanding model systems for atoms because μm-sized colloidal particles and their thermal motions can be directly visualised by optical microscopy and tracked by image analysis [8]. Various phase transitions have been studied at the single-particle level using colloids, such as crystallisation [9], melting [10, 11], sublimation [12], condensation [13], glass transition [14] and s–s transition [15, 16]. In recent years, colloidal particles with temperature-sensitive attractions have been fabricated [12, 17–19]. It opens the way to study the free surfaces of solids, i.e. crystal–vapour interfaces. In contrast, repulsive particles cannot form free surfaces at thermal equilibrium. The surface premelting with single-particle dynamics was previously reported in

ref. [17]. Here, we discover pre-s–s transition in a similar colloidal suspension of poly(methylmethacrylate) (PMMA) spheres in an aqueous black dye. We also use a colloidal suspension of thermosensitive N-isopropyl acrylamide-metharylamide (NIPA) microgel spheres in a red dye. The strengths of the dye-induced attractions in PMMA and NIPA colloids change in opposite directions with temperature, and both can be finely tuned at approximately 30°C (Fig. S2). When confined between two plates, PMMA and NIPA spheres exhibit similar phase behaviors as hard spheres, including monolayer triangular lattice (1△), two-layer square lattice (2□), $2\triangle, 3\square, 3\triangle, 4\square, \cdots$ phases, as the wall separation H increases [20, 21] (Fig. S1c). Similar phases have also been discovered in plasma [22] and in the electron bilayers of semiconductors [23]. Experimental details are provided in Methods.

Surface crystals at equilibrium

We observe the 4□ lattice formed on the surface of a 4△ PMMA colloidal crystal (Fig. 1d-i) by lowering the temperature, as this weakens the inter-particle attractions and thus increases the effective temperature (path 1 in Fig. S1d). A premelted liquid layer observed by ref. [17] does not form, because the temperature and wall separation are closer to the 4△–4□ transition than the 4△–liquid transition. The □ and △ crystals have the same lattice constant; consequently, a coherent □–△ interface can form along their (10) directions (Figs. 1e–g). This is in accordance with our observation that a 4□ crystal can only form on free surfaces along the (10) direction of a 4△ crystal (Fig. S5). Quasistatic cooling generates 4□ crystals of thickness $l \propto (T - T_{\text{s-s}})^{-\alpha}$ (Fig. 1d). Such power-law divergence has been predicted by premelting theory [1, 24], and has been observed in simulations [25] and experiments on the premelting of metals [26] and this PMMA colloidal system [17]. This further confirms that the pre-s–s transition and premelting have the same mechanism.

The kinetic processes of the surface crystal formation are shown in Figs. 1e–i, Fig. S3, Movie 1 and Movie 2. Small □-lattice crystallites randomly nucleate at the △-lattice surface, and then grow laterally until the entire surface is covered (Figs. 1e, f). As the temperature decreases (i.e. the effective temperature increases), a 4□ lattice grows into the bulk △-lattice by bending local △-lattices, and then swiftly transforms into □-lattices (Figs. 1g–i, Movie 2). These collective motions of tens of particles represent a martensitic transition, and are probably generated by anisotropic stress near the surface. Specifically, the weakened attraction between particles leads to a slight expansion of the 4△ crystal, enabling it to freely expand towards the liquid phase, but this also induces a stress tangential to the surface. This stress is relieved by the bending of local △-lattices, which preserves the local coherent □–△ interface. The accumulated stress eventually leads to abrupt fracturing of the coherent interface, resulting in many defects (Fig. 1i).

We observe similar 4□ surface crystals on the NIPA colloidal crystals. Both liquid–□ and □–△ interfaces form steps, and transformations occur at kinks (Fig. 1j). In $4\triangle \rightarrow 4\square$ crystals, particles at the interface collectively shift row-by-row by less than one lattice constant, without generating obvious lattice distortions (Movie 3). This is probably because NIPA, being softer than PMMA, can better relax local stresses.

Reversing the temperature change causes the surface □ crystal to transform back into the bulk △ crystal via row-by-row shifts of particles from kinks in PMMA colloids (Fig. S4 and Movie 4). The □ lattice is less dense than the △ lattice, hence there is sufficient space for particles to collectively move row-by-row in a $\square \rightarrow \triangle$ transition without generating the local distortions and stresses seen in a $\triangle \rightarrow \square$ transition in Figs. 1g–i. Irreversible kinetics are common in s–s transitions, due to complex stresses dominating the kinetic pathways [27]. For soft NIPA crystals, $\triangle \rightarrow \square$ and $\square \rightarrow \triangle$ processes are reversible with similar row-by-row transformations.

The surface crystals are sometimes polycrystalline. This is due to □-crystal growth from zigzag facets in the initial vapour–△ interface (Fig. S5b), or to substantial temperature changes generating bulk expansion that distorts the surface into a polycrystal.

We also perform molecular dynamics simulations of particles with the 12-6 Lennard-Jones (LJ) potential to confirm the existence of surface crystals, as detailed in the Methods. As the temperature increases quasistatically, the bulk $n\triangle$ crystal develops a surface $n\square$ crystal whose thickness $l \sim (T_{\text{s-s}} - T)^{-\alpha}$ for $n = 3, 4$ (Fig. 1k). Thus, power-law behaviour holds in the simulations and experiments with different particle interactions and different thicknesses of crystalline films. The kinetics after an abrupt temperature change are shown in Figs. 1l–n. First, a few layers of particles near the free surface become highly mobile liquid-like and nucleate into small □ crystallites. These □ lattices grow to completely cover the entire surface. Such early-stage kinetics are similar to that observed in colloid experiments (Figs. 1e, f), while the latter-stage kinetics involve row-by-row $\triangle \rightarrow \square$ transformations (Fig. 1n, Fig. S8) as illustrated by the particles' displacements in Fig. 1o. The slightly different kinetics between the simulation and PMMA colloid experiment may be attributable to different particle interactions and imperfections in the colloidal crystals. For example, the defects and stepped interfaces in Fig. 1 could interrupt the row-by-row transformation, thereby generating local lattice distortions.

The reverse $4\triangle \rightarrow 4\square$ process involves a similar row-by-row transformation (Fig. 1o, Fig. S10) and yields the same $l(T)$ without hysteresis (Fig. 1k). Such reversibility confirms that the surface crystal formation is a wetting phenomenon that occurs at thermal equilibrium, rather

than a first-order transition that occurs via nucleation. Note that it can neither be a continuous phase transition as the two crystals have distinct densities.

The hard-sphere phase diagram (Fig. S1c) shows that an $n\square$ crystal can transform into an $n\triangle$ or $(n-1)\triangle$ crystal. However, we do not observe pre-s–s surface crystal formation during these transitions, which can be explained as follows. The free surface of an $n\square$ crystal cannot develop an $n\triangle$ wetting layer because the density of an $n\triangle$ crystal is greater than that of an $n\square$ crystal, and thus vapour–$n\triangle$ interfacial energy is higher than vapour–$n\square$ interfacial energy. The free surface of an $n\square$ crystal can neither develop a surface $(n-1)\triangle$ crystal, because the one-layer mismatch in the z-direction means that a fully coherent interface cannot form.

Transient surface crystals

Surface crystals can also affect nonequilibrium processes, such as polycrystal annealing, melting and crystallisation. For example, during the annealing of the $4\triangle$ polycrystal in Fig. 2, $4\square$ crystals form at the ends of high-angle (mismatch angle $\theta = 30°$) grain boundaries (GBs), because this makes all of the $\square$–$\triangle$ interfaces coherent and thus lowers the energy of the original GBs. These $4\square$ crystals increase in size, which brings the neighboring GBs closer (Fig. 2b). A $4\square$ lattice band forms between these two GBs, as their coherent interfaces effectively reduce the energies of the two high-angle GBs (Fig. 2c, Fig. S11c, Movie 5). Particles on the coherent interfaces can easily shift slightly row-by-row without inducing much stress, thus facilitating GB coalescence (Fig. S12). $4\square$ lattices form at the GB–surface junctions of GBs with $\theta = 20°$, but no $4\square$ band forms between these two GBs because not all of the $\square$–$\triangle$ interfaces can be coherent simultaneously (Fig. S13). Low-angle GBs ($\theta < 15°$) coalesce directly, without the intermediacy of $\square$ lattices (Fig. S14), because their energies are already low. Similar to these simulation results for LJ particles, the NIPA colloid experiments also show that $4\square$ surface crystals can form at high-angle GBs (Figs. 2e–g), but not at low-angle GBs (Fig. S6). However, a single $4\square$ crystal can form coherent interfaces with both $4\triangle$ grains across a 20° GB via deformed rhombic lattices (Fig. 2f), probably because the NIPA crystal is more deformable than the LJ crystal.

We observed that a polymorphic surface crystal can temporarily form during bulk crystal melting. When the temperature is rapidly increased above the $n\triangle$ melting point (path 2 in Fig. S1d), the $n\triangle$ lattice converts to an $n\square$ crystal via collective row-by-row transformation, and the other side of the $n\square$ crystal melts. Eventually, all of the $\square$ and $\triangle$ crystals melt, as shown in the experimental data (Figs. 3a-c and Movie 6) and the simulation data (Fig. S15). Similarly, if the temperature is rapidly decreased below the $n\triangle$ freezing point, the liquid solidifies to a $4\square$ crystal, and then its other side transforms layer-by-layer into a $4\triangle$ crystal (Fig. 3d-f). During this process, the $4\triangle$ bulk crystal grows, while the thickness of the surface $4\square$ remains nearly constant (Movie 7). Surface crystal observed in crystallisation has been interpreted as a transient wetting layer [28] which will vanish after the crystallisation. By contrast, if the supercooling temperature is close to the s-s transition point, the wetting layer is a pre-s-s transition which will not vanish after the crystallisation.

Premelting and prefreezing are opposite phenomena. Similarly, the opposite phenomenon to the pre-s–s transition of a low-density surface crystal is the formation of a high-density polymorphic crystal on the surface of a low-density crystal. This is possible at the bulk crystal–substrate interface, but not at the bulk–vapour or bulk–liquid interfaces. Specifically, if a solid substrate has a lower affinity for a bulk crystal than for a polymorphic crystal, an interfacial wetting layer of polymorphic crystal can form on the substrate before it reaches the s–s transition point, similar to prefreezing.

Double surface layers at equilibrium

Premelting, prefreezing and pre-s–s transitions all involve one surface wetting layer. In addition, we propose that double-surface wetting layers can exist, i.e. superpositions of premelting and pre-s–s transitions (Fig. S1e). For example, the surface of a bulk $\triangle$ lattice can develop a $\square$ layer and a liquid layer if the vapour–$\triangle$–$\square$ triple-point is close to the vapour–liquid–$\square$ triple-point, such that $\gamma_{\text{vapour–}\triangle} > \gamma_{\text{vapour-liquid}} + \gamma_{\text{liquid–}\square} + \gamma_{\square\text{–}\triangle}$. This theoretical expectation is confirmed in experiments (Fig. 4a) and simulation (Fig. 4b) at appropriate wall separations. The double wetting layers in Fig. 4 are not a transient phenomenon, as they remain stable after a long period of equilibration (Movie 8). Both surface layers grow as the temperature quasistatically changes within a narrow temperature range, which is consistent with the above theoretical expectation that double layers can only exist near both triple points.

Discussion

We propose two novel surface-wetting phenomena: (1) the formation of a polymorphic crystalline layer on the surface of a bulk crystal in vapour or liquid, i.e. a pre-s–s transition; and (2) the formation of a double surface layer of liquid and polymorphic crystal when the melting and s–s transition points (i.e., triple points) are close. The existence of these phenomena is confirmed by colloid experiments and simulations of 12-6 LJ and 16-8 LJ potentials (Fig. S16). The power-law of the surface-layer thickness $l(T)$ is in accordance with the premelting theory, and holds for different particles and film thicknesses. However, the formation kinetics depend on surface morphology and particle interaction. The surface crystal grows from the bulk crystal side, rather than from the vapour or liquid side, in accordance with a pre-s–s tran-

sition process rather than a vapour- or liquid-deposition process.

Note that a 4□ crystal on the surface of a 4△ crystal does not represent an s–s coexistence phase in which the two crystals have the same chemical potential. Otherwise, the system would be at the vapour–4△–4□ triple-point, and such a three-phase coexistence could not be maintained when the temperature changed. This is explained by the phase rule [29], which states that three phases in a single-component system can coexist only at a fixed temperature and pressure (see Fig. S1d and discussions). Analogously, the double surface layers in Fig. 4 represent a surface phenomenon at thermal equilibrium, rather than the coexistence of four-phases.

Surface crystals occur when two polymorphic crystals can form a coherent interface. Coherent interfaces play important roles in semiconductors and superconductors [30], but they are mainly formed between crystals with different compositions. Most polymorphic crystals cannot form coherent interfaces, which is probably the reason that surface-crystal phenomenon has not been reported before. To guide the search of the surface-crystal phenomenon, we suggest two examples of polymorphic crystals that can form coherent interfaces: lonsdaleite (i.e. hexagonal diamond) and graphite [31], and anatase and TiO_2(B) (Fig. S17) [32]. Thus, the free surface of high-density lonsdaleite (or anatase) can transform into a layer of low-density graphite (or TiO_2(B)) before reaching the s–s transition point. Lonsdaleite-silicon [33] and silicene [34], which are the silicon analogues of the above carbon allotropes, can also form a coherent interface, and thus may also be capable of forming surface polymorphic crystals.

These temperature-controlled surface layers provide a simple method for tuning crystal properties. As a similar phenomenon, surface reconstruction has various implications in controlling materials' chemical, catalysis, adhesion, mechanical, electrical, magnetic and optical properties [7]. In contrast to surface reconstruction with only one or a few layers of atoms which are not thermally tuneable, the pre-s-s phenomenon exhibits a much thicker and tuneable surface layer which will not be worn out, and thus could better control the surface properties. Moreover, surface polymorphic crystals can exist during bulk crystal melting or crystallisation, and alter the rates of these processes. Surface crystals can also facilitate polycrystalline grain coarsening, which could be useful in materials fabrication.

Methods

Experiments

The first colloidal system is an aqueous suspension of PMMA spheres with a mean diameter of $\sigma = 2.02$ μm and a polydispersity of less than 5% [17]. The suspension is composed of 77% water and 23% nonfluorescent liquid dye (D98010 Chromatint jet black 1990, Chromatech Incorporated), i.e. 4 wt% solid dye after drying. The dye solution is heated for 5 h at 60°C, and then ultrasonicated for 1 min at room temperature.

The pair potential $U(r)$ in Fig. S2B is derived from the radial distribution function $g(r)$ of a monolayer of colloidal gas at equilibrium [35]. The radial distribution function $g(r = |\vec{r}|) = \frac{1}{n^2}\langle\rho(\vec{r'} + \vec{r}, t)\rho(\vec{r'}, t)\rangle$, where n is the area density, ρ is local number density and $\vec{r}$ is the particle position. $U(r)$ is derived from $g(r)$ by the Ornstein–Zernike integral equation using the Percus–Yevick approximation or a hypernetted-chain approximation [35, 36]. The two methods yield the same result, suggesting that the measured $U(r)$ is accurate. The colloidal particles with relatively long-range attractive forces can better mimic atoms than purely repulsive colloidal particles. The shape- and concentration-dependence of $U(r)$ [17] suggest that it could be a depletion attraction [37] induced by large clusters of dye molecules [38]. The effective temperature k_BT/U_{min} is dominated by the attraction depth U_{min}, as T only changes slightly near 300 K during our experiment. PMMA spheres can form crystals even at low temperatures, where the attraction of $U(r)$ is weak. This indicates that the inter-particle attraction is stronger in colloidal crystals than the $U(r)$ measured in the dilute gas phase, in accordance with the fact that the depletion force is non-pairwise additive, and that many-body effects could enhance the attraction.

The second colloidal system is an aqueous suspension of NIPA (or pNIPAM) spheres that have a small methacrylamide core [39]. Their diameters are approximately 1 μm with 3% polydispersity, and change with temperature. The suspension also contains 1.4 wt% non-fluorescent red dye (Chromatech-Chromatint Red 1064 Liquid, Chromatech Incorporated) [40] at pH = 5. Temperature-sensitive attractions can be induced between PMMA spheres by the black dye, and between the NIPA spheres by the red dye, as indicated by their pair potentials $U(r)$ shown in the Fig. S2. Moreover, a third attractive colloidal system can be generated without dye: attractions can exist between NIPA spheres in the absence of red dye if the pH is set to 10 by the addition of NaOH, which is probably due to hydrogen bonding in such alkaline solution [41]. However, these attractions are not tuneable. Similarly, this type of dye-free system can also form surface 4□ crystals, akin to the above-mentioned dye-containing colloidal systems, but the formation processes and other kinetics are difficult to measure, due to their non-tuneable interactions. Although the mechanisms of the attractions for PMMA and NIPA colloid particles are not fully understood, the attractions themselves are well reproducible, and thus PMMA and NIPA colloids- are sufficiently robust for the study of surface phenomena.

We prepare thin-film samples as follows. A droplet of a colloidal suspension is placed on a glass slide, and then

covered with a glass coverslip. The glass slides and coverslips are pre-cleaned by sonication in a 1:4 solution of $H_2O_2 : H_2SO_4$ and flame treatment to prevent particles sticking to the glass surfaces. By adding an appropriate volume of the colloidal suspension, we can control the sample cell thickness H. For example, a 1.0 μL colloid usually forms four layers at the centre and six layers at the edges in an 18×18 mm^2 sample area. Therefore, the local thickness can be regarded as uniform over a ~ 100 μm field of view. The droplet spreads out over most of the coverslip area by capillary force, and the coverslip and the glass slide are then glued together with epoxy and hardened in air for 30 min to fix the wall separation. During the observation and video-recording, the temperature is tuned using a temperature controller (Bioptechs) attached to a 100× oil-immersion objective, and good thermal contact is achieved by the use of a ~ 1 cm^2 area of immersion oil. The $\sim 10^{-4}$ cm^2 field of view is in the centre of a ~ 1 cm^2 heated area, and thus the temperature in the field of view is uniform. In contrast, there is a temperature gradient at the edge of the heated area, which generates a thermophoretic effect [42] that pumps dye in or out of the heated area in response to increases or decreases in the temperature. The pumping drift ceases within 30 s of the application of temperature change, indicating that the dye distribution has reached a new steady state. Temperature changes sometimes cause a small drift of the suspension or an expansion of the crystal, and the whole crystal may oscillate with an amplitude of less than the size of one particle, but these motions are temporary, and do not affect the behaviour of surface layers.

Simulations

In most simulations, particles have a 12-6 LJ potential [43]:

$$V(r) = \epsilon \left[\left(\frac{\sigma}{r}\right)^{12} - 2\left(\frac{\sigma}{r}\right)^{6} \right] + f(r), \qquad (2)$$

where r is the interparticle separation and σ is the effective diameter. $f(r)$ is set such that $U(r = 2.5\sigma) = 0$ and $U(r > 2.5\sigma)$ is set as 0 [44]. The units of length, mass and energy are the particle diameter σ, mass m and characteristic energy ϵ, respectively. Accordingly, the units of time and temperature are $\tau = \sqrt{m\sigma^2/\epsilon}$ and ϵ/k_B, where k_B is the Boltzmann constant. The time step is set to be 10^{-3}. The LJ potential is the most widely used potential in simulations and can well describe the interactions between electronically neutral atoms or molecules. 16-8 and 12-9 LJ potentials can be similarly defined based on their power law exponents. The interaction potential between a particle and a wall in the z direction $U(r) = 12000\times(r-0.5)^2$; this potential is steep, and can represent a hard wall. Similar to hard spheres, LJ particles also form a cascade of several-layer □ and △ lattices at different wall separations, although a quantitative phase diagram for thin-film confinement has not been determined in literature. Our simulation of particles with a 16-8 LJ potential with the cut-off length 2.5σ produces similar results (Fig. S16).The 16-9 LJ potential also has a cut-off length 2.5σ which can form double surface layers relatively easily.

The simulations are performed in the NVT ensemble with a Nose–Hoover thermostat, a constant number of particles N and at a constant volume V and temperature T, in an $L_x \times L_y = 30 \times 160\sqrt{3}$ rectangular box containing 4,800 particles per layer under periodic boundary conditions. The whole system is shown in Fig. S7. We set $H = 2.64, 3.46$ for three- and four-layer samples, respectively. The equilibration time becomes extremely long near $T_{s\text{-}s}$ because the chemical potentials of the □ and △ crystals are very close. To reach full equilibration, we run 2×10^6 time steps at each temperature with $\Delta T = 0.01$/step from $T = 0$ to 0.485, and run 5×10^8 time steps with $\Delta T = 0.001$/step at each temperature near $T_{s\text{-}s}$.

[1] Dash, J. G., Rempel, A. W. & Wettlaufer, J. S. The physics of premelted ice and its geophysical consequences. *Rev. Mod. Phys.* **78**, 695-741 (2006).

[2] Slarter, B. & Michaelides, A. Surface premelting of water ice. *Nat. Rev. Chem.* **3**, 172-188 (2019).

[3] Heni, M. & Lowen, H. Surface freezing on patterned substrates. *Phys. Rev. Lett.* **85**, 3668-3671 (2000).

[4] Auer. S & Frenkel. D. Line tension controls wall-induced crystal nucleation in hard-sphere colloids. *Phys. Rev. Lett.* **91**, 015703 (2003).

[5] Dijkstra, M. Capillary freezing or complete wetting of hard spheres in a planar hard slit? *Phys. Rev. Lett.* **93**, 108303 (2004).

[6] Wu, X. Z., Ocko, B. M., Sirota, E. B., Sinha, S. K., Deutsch, M., Cao, B. H. & Kim, M. W. Surface tension measurement of surface freezing in liquid normal alkanes. *Science* **261**, 1018-1021 (1993).

[7] Somorjai, G. A. Surface reconstruction and catalysis. *Annu. Rev. Phys. Chern.* **45**, 721-751 (1994).

[8] Li, B., Zhou, D. & Han, Y. Assembly and phase transitions of colloidal crystals. *Nat. Rev. Mater.* **1**, 15011 (2016).

[9] Gasser, U., Weeks, E. R., Schofied, A., Pusey, P. N. & Weitz, D. A. Real-space imaging of nucleation and growth in colloidal crystallization. *Science* **292**, 258-262 (2002).

[10] Alsayed, A, M., Islam, M. F., Zhang, J., Collings, P. J. & Yodh, G. Premelting at defects within bulk colloidal crystals. *Science* **309**, 1207-1210 (2005).

[11] Wang, Z., Wang, F., Peng, Y., Zheng, Z. & Han, Y. Imaging the homogeneous nucleation during the melting of superheated colloidal crystals. *Science* **338**, 87-99 (2012).

[12] Savage, J. R., Blair, D. W., Levine, A. J., Guyer, R. A. & Dinsmore, A. D. Imaging the sublimation dynamics of colloidal crystallites. *Science* **314**, 795-798 (2006).

[13] Nguyen, V., Faber, S., Hu, Z., Wegdam, G. & Schal-

l, P. Controlling colloidal phase transitions with critical Casimir forces. *Nat. Commun.* **4**, 1584 (2013).
[14] Weeks, E. R., Crocker, J. C., Levitt, A. C., Schofield, A. & Weitz, D. A. Three-dimensional direct imaging of structural relaxation near the colloidal glass transition. *Science* **28**, 627-631 (2000).
[15] Peng, Y., Wang, F., Wang, Z., Alsayed, A. M., Zhang, Z., Yodh, A. G. & Han, Y. Two-step nucleation mechanism in solid-solid phase transitions. *Nat. Mater.* **14**, 101 (2015).
[16] Casey, M. T., Scarlett, R. T., Rogers, W. B., Jenkins, I., Sinno, T. & Crocker, J. C. Driving diffusionless transformations in colloidal crystals using DNA handshaking. *Nat. Commun.* **3**, 1209 (2012).
[17] Li, B., Wang, F., Zhou, D., Peng, Y., Ni, R. & Han, Y. Modes of surface premelting in colloidal crystals composed of attractive particles. *Nature* **531**, 485-488 (2016).
[18] Hertlein, C., Helden, L., Gambassi, A., Dietrich, S. & Bechinger, C. Direct measurement of critical Casimir forces. *Nature* **451**, 172-175 (2008).
[19] Rogers, W. B. & Manoharan, V. N. Programming colloidal phase transitions with DNA strand displacement. *Science* **347**, 639-642 (2015).
[20] Fortini, A. & Dijkstra, M. Phase behaviour of hard spheres confined between parallel hard plates: manipulation of colloidal crystal structures by confinement. *J. Phys. Cond. Matt.* **18**, L371-L378 (2006).
[21] Schmidt. M & Lowen, H. Freezing between two and three dimensions. *Phys. Rev. Lett.* **76**, 4552-4555 (1996).
[22] Mitchell, T. B., Bollinger, J. J., Dubin, D. H. E., Huang, X. P., Itano, W. M. & Baughman, R. H. Direct observations of structural phase transitions in planar crystallized ion plasmas. *Science* **282**, 1290-1293 (1998).
[23] Narasimhan, S. & Ho, T. L. Wigner-crystal phases in bilayer quantum Hall systems. *Phys. Rev. B* **52**, 12291-12306 (1995).
[24] Lipowsky, R. Critical surface phenomena at first-order bulk transitions. *Phys. Rev. Lett.* **49**, 1575-1577 (1982).
[25] Broughton, J. Q. & Gilmer, G. H. Interface melting: simulations of surfaces and grain boundaries at high temperatures. *J. Phys. Chem.* **91**, 6347-6359 (1987).
[26] Frenken, J. W. M. & van der Veen, J. F. Observation of surface melting. *Phys. Rev. Lett.* **54**, 134-137 (1985).
[27] Porter, D. A., Easterling, K. E. & Sherif, M. Y. *Phase Transformations in Metals and Alloys* (CRC Press, Boca Raton, 2008).
[28] S. Arai, H. Tanaka, *Nat. Phys.* **16** , 503-509 (2017).
[29] Gibbs, J. W. *Scientific Papers: Thermodynamics Vol.* (Dover Publications, New York, 1961).
[30] Qi, X. & Zhang, S. Topological insulators and superconductors. *Rev. Mod. Phys.* **83**, 1057-1110 (2011).
[31] Xie, Y. P., Zhang, X. J. & Liu, Z. P. Graphite to diamond: origin for kinetics selectivity. *J. Am. Chem. Soc.* **139**, 2545-2548 (2017).
[32] Wang, C., Zhang, X. & Liu, Y. Coexistence of an anatase/TiO_2(B) heterojunction and an exposed (001) facet in TiO_2 nanoribbon photocatalysts synthesized *via* a fluorine-free route and topotactic transformation. *Nanoscale* **6**, 5329-5337 (2014).
[33] Wentorf Jr., R. H. & Kasper, J. S. Two new forms of silicon. *Science* **139**, 338-339 (1963).
[34] Aufray, B., Kara, A., Vizzini, S., Oughaddou, H. et al. Graphene-like silicon nanoribbons on Ag(110): A possible formation of silicene. *Appl. Phys. Lett.* **96**, 183102 (2010).
[35] Behrens, S. H. & Grier, D. G. Pair interaction of charged colloidal spheres near a charged wall. *Phys. Rev. E* **64**, 050401 (2001).
[36] Polin, M., Grier, D. G. & Han, Y. Colloidal electrostatic interactions near a conducting surface. *Phys. Rev. E* **76**, 041406 (2007).
[37] Louis, A., Allahyarov, E., Lowen, H. & Roth, R. Effective forces in colloidal mixtures: From depletion attraction to accumulation repulsion. *Phys. Rev. E* **65**, 061407 (2002).
[38] Horowitz, V. R., Janowitz, L. A., Modic, A. L., Heiney, P. A. & Collings, P. J. Aggregation behavior and chromonic liquid crystal properties of an anionic monoazo dye. *Phys. Rev. E* **72**, 041710 (2005).
[39] Asghar, K., Qasim, M., Dharmapuri, G. & Das, D. Investigation on a smart nanocarrier with a mesoporous magnetic core and thermo-responsive shell for co-delivery of doxorubicin and curcumin: a new approach towards combination therapy of cancer. *RSC Adv.* **7**, 28802-28818 (2017).
[40] Yunker, P., Zhang, Z., Aptowicz, K. B. & Yodh, A. G. Irreversible rearrangements, correlated domains, and local structure in aging glasses. *Phys. Rev. Lett.* **103**, 115701 (2009).
[41] Kokufuta, E. Polyelectrolyte gel transitions:? Experimental aspects of charge inhomogeneity in the swelling and segmental attractions in the shrinking. *Langmuir* **21**, 10004-10015 (2005).
[42] Jiang, H. R., Wada, H., Yoshinaga, N. & Sano, M. Manipulation of colloids by a nonequilibrium depletion force in a temperature gradient. *Phys. Rev. Lett.* **102,** 208301 (2009).
[43] Wang, X. Ramrez-Hinestrosa, S. Dobnikar, J & Daan, F. The Lennard-Jones potential: when (not) to use it. *Phys. Chem. Chem. Phys.* **22,** 10624-10633 (2020).
[44] Frenkel, D. & Smit, B. *Understanding Molecular Simulation: From Algorithm to Applications* (Academic Press, San Diego, 2010).

Data availability

Source data support the plot are provided with this paper.

Code availability

The computer codes used in this paper are provided with this paper

Acknowledgements

We thank Daan Frenkel, Jure Dobnikar, Wei Li, Qi Zhang and Kaiyao Qiao for useful discussions, Xinliang Xu for part of the computational facility, and Yongjun Zhang and Yafei Wang for the NIPA colloid. This work was supported by RGC-GRF grants nos. 16301117 and 16302518 and CRF-C6016-20G and NSFC grant no. 12104495.

Author information

These authors contributed equally: Xipeng Wang, Bo Li.

Corresponding author

Correspondence to Yilong Han: yilong@ust.hk.

Author contributions

Y.H. and B. L. proposed the existence of the surface-crystal phenomena. Y.H., B.L. and X.W. conceived and designed the research. X.W. carried out the simulations. B.L. and M.L. conducted the experiments with PMMA and NIPA colloids, respectively. B.L., X.W. and M.L. analysed the data, with help from Y.H. X.W., Y.H. and B.L. wrote the paper. Y.H. supervised and supported the work. All authors discussed the results.

Competing interest The authors declare no competing interests.

Additional information

Supplementary information includes Figs. S1-17, Discussion and Movies 1-8.

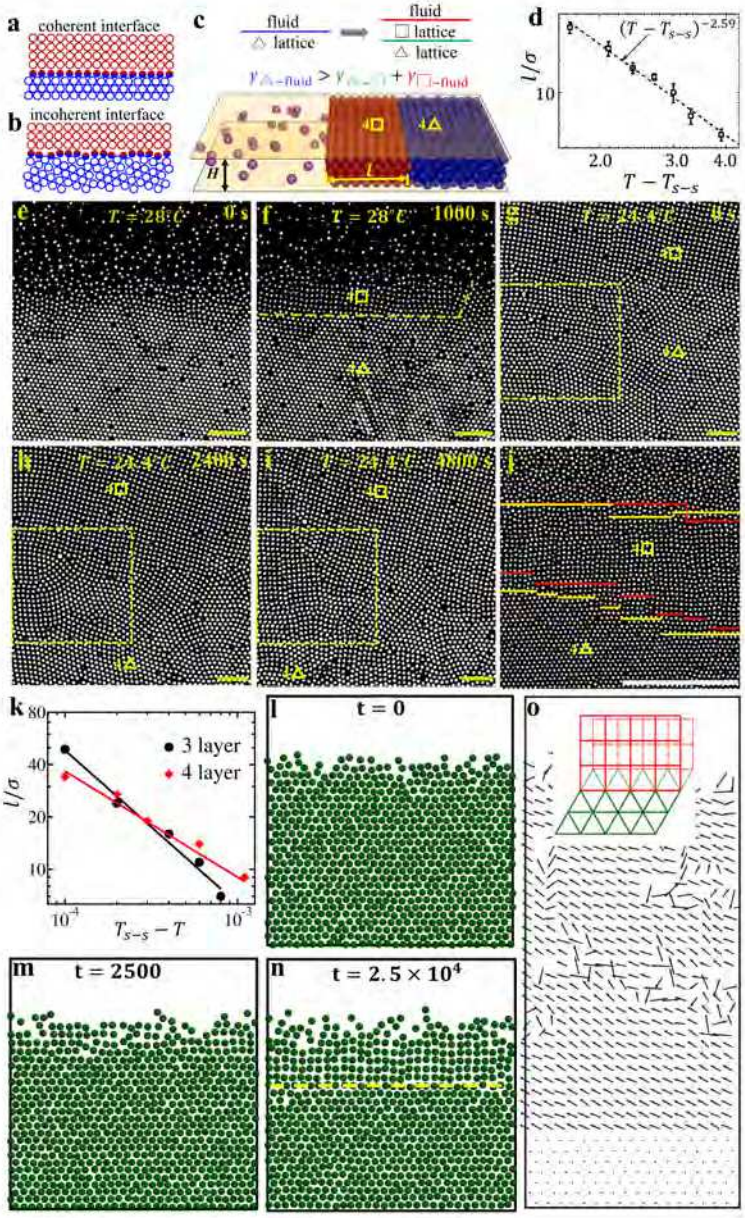

FIG. 1: **A** 4□ **crystal on the surface of a bulk** 4△ **crystal. a,** A coherent interface between square and triangular lattices, where the row of half-red-half-blue particles on the interface match with both lattices. **b,** The two lattices do not match well, thereby forming an incoherent interface. **c,** A schematic of the sample. 4□ crystals at fluid–4△ interfaces in (d–i) a PMMA colloid, (j) a NIPA colloid and (k–o) a simulation. **d,** Thickness of the 4□ crystal at equilibrium fitted by $l \sim (T - T_{\text{s-s}})^{-\alpha}$ with $\alpha = 2.59$. The fitted $T_{\text{s-s}} = 23.6°\text{C}$ agrees well with the $T_{\text{s-s}}$ measured directly where the whole 4△ lattice transforms to a 4□ lattice. **e, f,** As the temperature decreases from 30.0°C to 28.0°C at $t = 0$, particles in the fluid phase nucleate into 4□ crystallites at the surface. **g–i,** 4△ → 4□ transformation after a thin 4□ layer covers the 4△ lattice as the temperature further decreases from 24.7°C to 24.4°C at $t' = 0$. A △ lattice in the boxed region collectively bends via an elastic affine deformation to a rhombic lattice in h, and then transforms swiftly into a □ lattice via a plastic deformation in i. **j,** In a NIPA colloid as T changes to 31.6°C, the liquid–□ and 4□–4△ interfaces (red lines) propagate to the yellow lines 10 min later. They form steps and grow from kinks, row by row. Scale bars: 20 μm. **k,** The equilibrium surface □ lattice thickness $l \sim (T_{\text{s-s}} - T)^{-\alpha}$ with the fitted $(T_{\text{s-s}}, \alpha) = (0.4891, 0.61)$ for 4□ crystals and $(0.4752, 0.89)$ for 3□ crystals. **l–n,** The kinetics after the temperature changes from 0.485 to 0.489 at $t = 0$. A few surface rows of 4△ particles melt, and then recrystallise into a 4□ lattice in M. **n,** The surface 4□ lattice grows into the bulk 4△ lattice. **o,** The displacement vectors of particles during the time interval $\Delta t = 30$ show the row-by-row growth depicted in the inset diagram. The initial and final positions are averaged over 1,000 steps in $\delta t = 10$ to remove thermal noise. The expansion of a low-density 4□ crystal generates a low concentration of vacancies. Only one layer in the xy-plane is shown in l–o; other layers in the z-direction are similar.

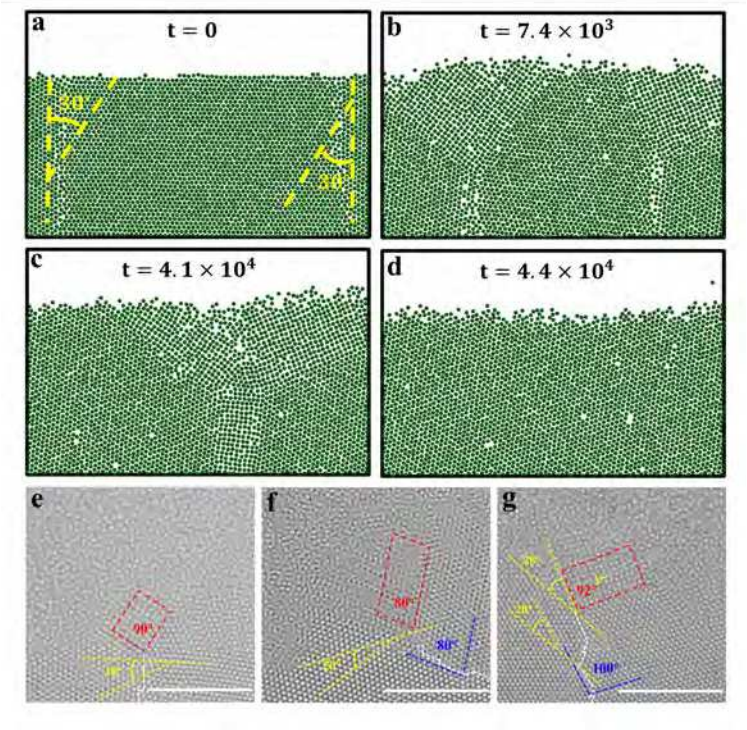

FIG. 2: 4□ **crystals at surface–GB intersections facilitate bulk polycrystal annealing in simulation (a to d) and form in NIPA colloids (e to g). a,** Two GBs with $\theta = 30°$. The temperature changes from 0.45 to 0.485 at $t = 0$. **b,** 4□ lattices form at the GB–surface intersections, attracting the two GBs closer together. **c**, When surface 4□ lattices coalesce, the middle 4△ grain shrinks and transforms into a 4□ band, see the full area in Fig. S11c. **d,** The 4□ lattices shrink, and ultimately transform into a single 4△ crystal. This confirms that the 4△ is the equilibrium phase and has the lowest chemical potential, and that the 4□ is an interfacial phenomenon. **e**, A single 4□ crystal forms coherent interfaces with both △-lattice grains, as the mismatch angle of the GB is 30°. Grain boundaries are labelled by white dashed lines. **f**, A 20° GB induces a rhombic lattice (red parallelogram) at the surface, such that the two $\triangle - \square$ interfaces remain coherent. **g**, The GB mismatch angle in the bulk is $120° - 100° = 20°$, but becomes 28° near the surface due to the slight deformation of the 4△ lattice. The surface 4□ domain contains a dislocation (⊥), and thus the nearby square lattice has an angle of 92° and forms two coherent $\triangle - \square$ interfaces. Scale bar: 20 μm.

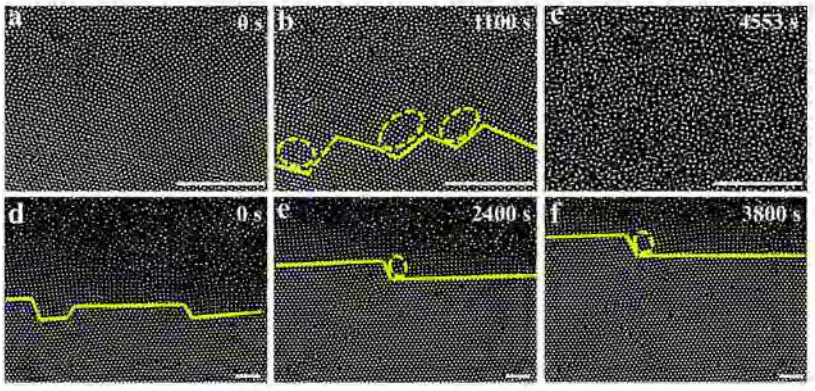

FIG. 3: **A transient surface** 4□ **crystal formed during the melting (a–c, NIPA colloid) and crystallisation (d–f, PMMA colloid) of a bulk** 4△ **crystal. a,** At $t = 0$, the temperature abruptly increases from 33°C to 34°C above the melting point. **b,** The surface 4□ lattice forms at $t = 1,100$ s. The solid and dashed line segments represent coherent and incoherent interfaces, respectively. **c,** By $t = 4,553$ s, the entire crystal in the field of view has melted; by $t = 5,500$ s, the entire crystal outside the field of view has melted. **d–f,** At $t = 0$, the temperature abruptly changes from 22°C to 27°C across the freezing point. **e,** The 4□ lattice maintains an approximately constant thickness, with one side growing from the fluid and the other side transforming layer-by-layer into a 4△ lattice. Deformed square lattice, i.e. rhombic lattices highlighted by ellipses, reduces the lattice mismatch near the kinks of the interfaces in b, e, f. Scale bar: 20 μm.

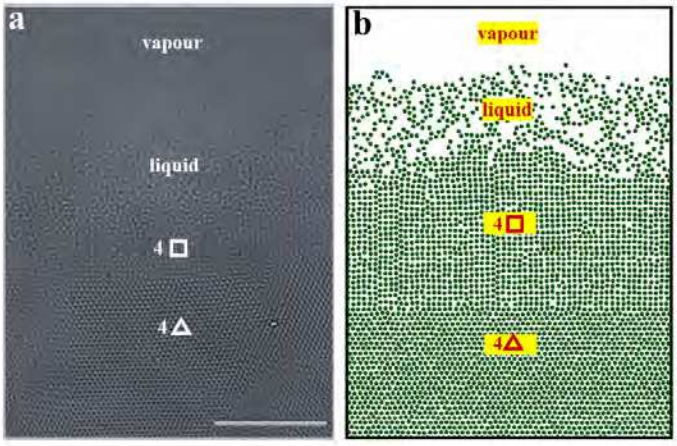

FIG. 4: **Double (□ and liquid) wetting layers at the interface of bulk △ crystal and vapour at thermal equilibrium. a,** Four layers (in z-direction) of NIPA colloidal particles at 32°C. Scale bar: 20 μm. **b,** Four layers of 12-9 LJ particles at $H = 3.45$ and $T = 0.484$ in a simulation.

Supplementary Files

This is a list of supplementary files associated with this preprint. Click to download.

- surfacecrystalSINM.pdf
- movie1.mp4
- movie2.mp4
- movie3.mp4
- movie4.mp4
- movie5.mp4
- movie6.mp4
- movie7.mp4
- movie8.mp4